Chinese Chemical Letters 36 (2025) 110383

Contents lists available at ScienceDirect

Chinese Chemical Letters

journal homepage: www.elsevier.com/locate/cclet

# Organocatalyzed iodine-mediated reversible-deactivation radical polymerization *via* photoinduced charge transfer complex catalysis

Xiang Li[a,1], Beibei Zhang[a,1], Zhixiang Wang[a,b,*], Xiangyu Chen[a,b,*]

[a] School of Chemical Sciences, University of the Chinese Academy of Sciences, Beijing 100049, China
[b] Beijing National Laboratory for Molecular Sciences, Beijing 100190, China

ARTICLE INFO

*Article history:*
Received 15 June 2024
Revised 19 August 2024
Accepted 29 August 2024
Available online 31 August 2024

*Keywords:*
*N*-Heterocyclic nitrenium salt
RDRP
Charge transfer complex
Visible light
Polymerization

ABSTRACT

Photoredox-mediated reversible-deactivation radical polymerization (RDRP) is an effective approach to synthesize polymers with defined composition and architecture. Current photoinduced RDRP primarily depends on outer-sphere electron transfer or homolysis mechanisms. Herein, we describe an example of iodine-mediated RDRP facilitated by photoinduced charge transfer complex (CTC) catalysis. The approach uses cheap and easily accessible N-heterocyclic nitrenium salt ($NHN^{+}\cdots I^{-}$) as the photoactive CTC. Upon the irradiation of visible light, $NHN^{+}\cdots I^{-}$ undergoes single electron transfer to generate NHN$^{\bullet}$ and I$^{\bullet}$ radicals. The NHN$^{\bullet}$ radical activates dormant $P_n$-I polymers *via* inner-sphere single electron transfer, leading to the propagating $P_n^{\bullet}$ radical for chain growth and the $I^{-}$ anion for recovering the CTC, and the I$^{\bullet}$ radical deactivates the polymerization *via* coupling with $P_n^{\bullet}$.



Reversible-deactivation radical polymerization (RDRP) has witnessed remarkable growth and is now recognized as one of the most versatile and widely used tool to synthesize polymers with well-defined structures and architectures, making it a potential technical for industrial applications [1–11]. Recently, organic photoredox catalysis offers a powerful approach to activate organic substrates, generating organic radicals for diverse transformations under mild and metal-free conditions [8,12]. This development has significantly advanced the progress of RDRP. In photoredox-mediated RDRP [13–22], the photocatalytic cycle usually proceeds *via* two pathways for the generation of propagating $P_n^{\bullet}$ and X$^{\bullet}$ radicals (Fig. 1A). The oxidative quenching pathway [23–26] relies on a strongly reducing excited PC$^{*}$ to achieve the single electron reduction of the dormant $P_n$-X polymers, resulting in $P_n^{\bullet}$ radical for propagation and a catalyst radical cation ($PC^{\bullet+}$) to oxidize the $X^{-}$ to X$^{\bullet}$ for the deactivation of the polymerization. However, organic PCs enabling such process have historically been rare [8,12,27–29]. In addition, the strong oxidizing power of $PC^{\bullet+}$ could lead to undesirable side reactions [26]. Alternatively, the reductive quenching pathway [30,31] in photoredox catalysis usually requires a stoichiometric amount of electron donors (*e.g.*, organic amine, $NR_3$) to reduce the excited PC$^{*}$, giving $PC^{\bullet-}$ and $NR_3^{\bullet+}$. The $PC^{\bullet-}$ then reduces $P_n$-X to $P_n^{\bullet}$ for propagation and $NR_3^{\bullet+}$ oxidizes $X^{-}$ to X$^{\bullet}$ for the deactivation of the polymerization. Recently, a consecutive photoinduced electron transfer strategy was successfully explored for photoinduced organocatalyzed atom transfer radical polymerization (ATRP) [32–34] in the presence of stoichiometry electron donors [35]. It is important to note that the photoinduced RDRP reactions of organic halides, such as photo-ATRP reactions, typically exhibit effective control over polymerization with Br and Cl chain end functionalities. The C-I bond tends to be unstable, leading to an inevitable degenerative transfer process that usually results in moderate control over polymerization [36,37]. Consequently, the use of alkyl iodides in ATRP is generally inefficient [38]. Nonetheless, for photocontrolled iodine-mediated RDRP, Goto, Kaji, and their colleagues have documented elegant photoinduced organocatalyzed reversible complexation-mediated polymerization (RCMP). In this process, dormant $P_n$-I polymers undergo homolysis in the presence of the catalyst, producing $P_n^{\bullet}$ and I$^{\bullet}$ radicals [39–42]. In this context, Cheng, Zhang and co-workers successfully employed solvent as halogen bonding acceptor to mediate the homolysis of $P_n$-I polymers (Fig. 1B) [43,44]. Furthermore, Matyjaszewski and co-workers reported an iodine-mediated photo-ATRP in aqueous media, where the alkyl iodide initiators are generated *in situ* from alkyl bromides [45].

Despite these advancements, current photoinduced RDRP primarily depends on outer-sphere electron transfer (OSET) or homolysis mechanisms. In contrast, the inner-sphere electron transfer (ISET) mechanism offers several advantages over OSET, such as

* Corresponding authors.
*E-mail addresses:* zxwang@ucas.ac.cn (Z. Wang), chenxiangyu20@ucas.ac.cn (X. Chen).
[1] These authors contributed equally to this work.

https://doi.org/10.1016/j.cclet.2024.110383
1001-8417/

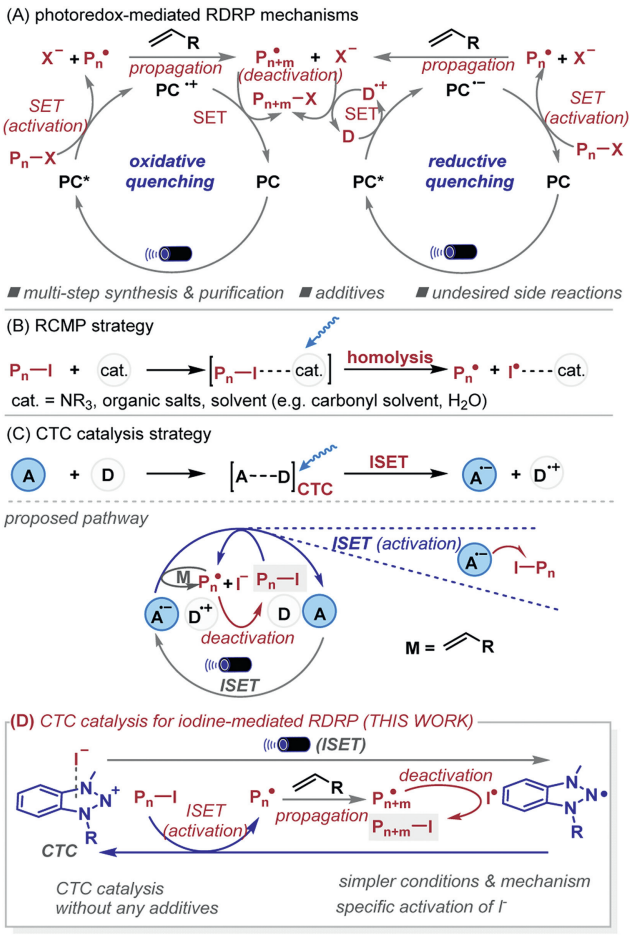


**Fig. 1.** (A) Photoredox-mediated RDRP mechanisms. (B) RCMP strategy. (C) Proposed pathway with CTC strategy. (D) Outline this work: CTC catalysis for iodine-mediated RDRP. See Fig. S13 (Supporting information) for the details of comparing the photo RCMP mechanism and our CTC catalysis. D: Electron donor.

independence from the reduction potential of the catalyst and reducing the side reactions [46]. We here quest whether the photoinduced intramolecular charge transfer complex (CTC) catalysis [47–50] can be applied for photocontrolled iodine-mediated RDRP *via* ISET.

Fig. 1C illustrates our hypothesis. Starting with the *in situ* formed CTC (denoted as D···A), the light excitation of the CTC generates $A^{\bullet-}$ and $D^{\bullet+}$ *via* single electron transfer (SET). The resultant $A^{\bullet-}$ then reduces the dormant $P_n$-I to $P_n^{\bullet}$ radical and $I^-$ which can be oxidized by $D^{\bullet+}$ to $I^{\bullet}$ for the deactivation of the polymerization. According to the mechanism, we further reasoned that, if the D···A uses $I^-$ as the electron donor of the CTC, this process would require no exogenous electron donor. Thus, a key to achieve the additive-free system is to identify a right CTC. Delightfully, our previous studies of the photocatalysis of *N*-heterocyclic nitreniums (NHNs) [51–59] inspired us. Previously, we have demonstrated that NHN salts can function as optimal CTC catalysts for the single-electron reduction of various organic halides through the ISET mechanism [60–65]. When exposed to visible light, the NHN salts could undergo charge transfer between the NHN cation and its counteranion or a sacrificial electron donor, resulting in an NHN aminyl radical species that could reduce the C-X bond. Thus, if the NHN salt uses $I^-$ as its counteranion (*i.e.*, $NHN^+\cdots I^-$ salt), the photoinduced iodine-mediated RDRP could proceed *via* the pathway shown in Fig. 1D, without using exogenous additive. As a result, it effectively minimizes side reactions and polymer contamination. Notably, the NHN salt is stable and can be easily prepared with one-step and commercially available starting materials. Very recently, Cheng, Zhang and co-workers developed an interesting near infrared photocontrolled iodine-mediated RDRP by employing persistent radical anions as the catalysts, which involves anion-$\pi$ complex ($I^-\cdots$PC) for the $I^{\bullet}$ radical and $PC^{\bullet-}$. However, this system still requires additional reducing agent and the alkyl iodide initiator was also generated by an *in-situ* halogen exchange from alkyl bromides [66–70].

**Table 1**
Optimization of the reaction conditions.[a]

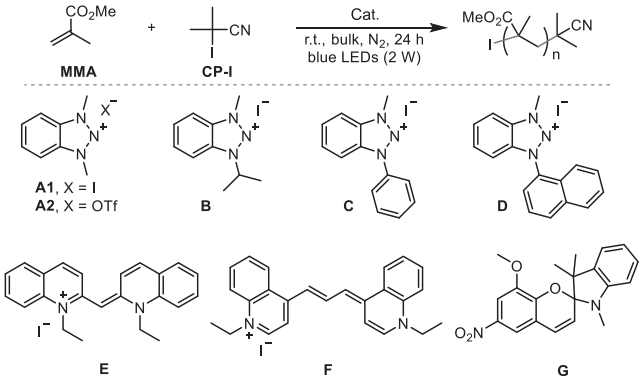


| Entry | Cat. | Conv. (%)[b] | $M_{n,GPC}$ (g/mol)[c] | $M_{w,GPC}$ (g/mol)[c] | $Đ$ ($M_w/M_n$)[c] | $I^*$ (%)[d] |
|---|---|---|---|---|---|---|
| 1 | **A1** | 89 | 20,200 | 24,700 | 1.22 | 89 |
| 2 | **B** | 51 | 10,800 | 13,800 | 1.28 | 96 |
| 3 | **C** | 32 | 7200 | 9000 | 1.25 | 92 |
| 4 | **D** | 49 | 10,200 | 12,400 | 1.22 | 98 |
| 5 | **A2** | Trace | 1500 | 1900 | 1.27 | – |
| 6[e] | **A1** | NR | – | – | – | – |
| 7 | **–** | NR | – | – | – | – |
| 8[f] | **A1** | NR | – | – | – | – |
| 9[g] | **A1** | 89 | 19,400 | 25,300 | 1.30 | 93 |
| 10[h] | **A1** | 66 | 13,700 | 17,300 | 1.26 | 97 |
| 11[h,i] | **A1** | 75 | 16,800 | 23,200 | 1.38 | 90 |
| 12 | NaI | 30 | 6900 | 8300 | 1.20 | 90 |
| 13 | $^nBu_4NI$ | 20 | 4400 | 5900 | 1.34 | 95 |
| 14 | **E** | 20 | 4500 | 7800 | 1.73 | 93 |
| 15 | **F** | 55 | 7400 | 11,900 | 1.61 | 151 |
| 16 | **G** | 12 | 2900 | 5700 | 1.28 | 90 |

[a] Reaction conditions: [MMA]:[CP-I]:[Cat.] = 200:1:0.2, room temperature (25 ± 5 °C), 455 nm LED (2 W), 24 h, bulk polymerization.
[b] Monomer conversion measured by $^1$H NMR.
[c] Molecular weights and molecular weight distributions were determined by GPC using PMMA as the standard in THF.
[d] $I^* = M_{n,theo}/M_{n,GPC}$, $M_{n,theo} = MW_{CP\text{-}I} + 200 \times MW_{MMA} \times$ Conversion%.
[e] Without initiator.
[f] Without light.
[g] [NHN **A1**]:[MMA] = 1:600.
[h] [NHN **A1**]:[MMA] = 1:2000.
[i] The reaction time is 36 h.

To validate the feasibility of our method, NHNs **A-D** were employed in the bulk polymerization of methyl methacrylate (MMA) with 2-cyanopropyl iodide (CP-I) [71–75] as the initiator. Our exploration of this transformation led us to identify suitable reaction conditions (Table 1). Specifically, using only 1/1000 catalyst loading of NHN **A1** (relative to monomer) under blue LED illumination afforded the desired polymer in a well-controlled manner ($Đ = 1.22$), with initiator efficiency $I^* = 89\%$ at 89% conversion (entry 1). Increasing or decreasing catalyst loading delivered inferior results in terms of conversion and dispersity (entries 9 and 10). Compared to entry 10, when prolonging the reaction time from 24 h to 36 h, the conversion increased by only 9% (entry 11). This slowdown in conversion can be attributed to the gradual decrease in polymerization rate during the later stage of the process. Other NHNs **B-D** also

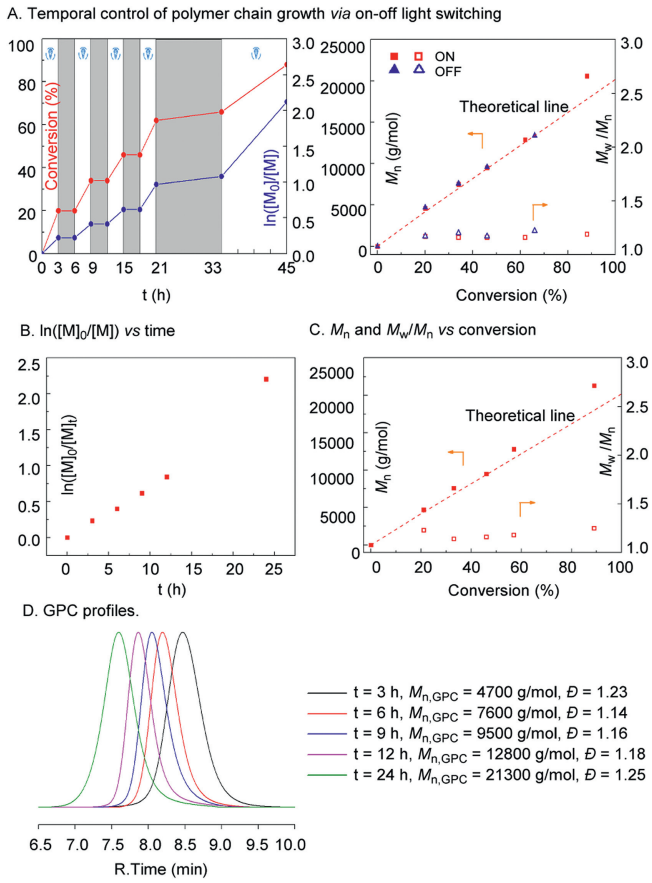


**Fig. 2.** Conditions: [Monomer]:[CP-I]:[NHN **A1**] = 200:1:0.2, room temperature, 455 nm LED (2 W), bulk polymerization. (A) Polymerization of MMA with NHN **A1** while switching the light irradiation between "ON" and "OFF" states. (B) $M_n$ and $M_w/M_n$ *vs.* conversion. (C) $\ln([M]_0/[M])$ *vs.* time. (D) GPC profiles of PMMAs correspond to different polymerization times for photoinduced CTC-catalyzed iodine-mediated RDRP of MMA.

gave good results albeit with lower conversions (entries 2–4). We attribute this to the greater steric hindrances of NHNs **B**-**D** compared to NHN **A1**, which likely results in weaker charge transfer abilities and consequently lower conversion rates [60-65]. Notably, only trace amounts of polymer were observed when $OTf^-$ (**A2**) was employed instead of $I^-$ as the counterion (entry 5), suggesting the crucial role of $I^-$ as the electron donor. Control experiments confirmed the necessity of the catalyst NHN **A1**, the initiator and blue light (entries 6–8). Notably, catalysts for RCMP proved ineffective under our present conditions (entries 12–16). The polymerizations performed in various solvents or with different light sources gave inferior results (Tables S2 and S3 in Supporting information).

The temporal control of the polymerization was investigated by toggling the light on and off. The results in Fig. 2A revealed that the polymerization nearly ceased when the light was off, and monomer conversion escalated during light exposure. Notably, during a 12 h dark interval (21–33 h), monomer conversion increased by only 4%. This minor increase is likely due to partial polymerization of monomers at room temperature in the absence of an inhibitor. Furthermore, the results in Fig. 2B indicated that the first-order plot of the monomer concentration [M] remained nearly linear within the studied time range. The change of $M_{n,GPC}$ and $M_w/M_n$ values with monomer conversion (Fig. 2C), as well as symmetrical GPC traces (Fig. 2D), further verified the living features of the polymerization system.

Next, we applied this method to the polymerization of a variety of monomers, including 2-methoxyethyl methacrylate (MEMA), 2,2,2-trifluoroethyl methacrylate (TFEMA), 2-ethylhexyl methacrylate (EHMA), benzyl methacrylate (BnMA), phenyl methacrylate (PhMA), 2-(dimethylamino)ethyl methacrylate (DMAEMA), butyl methacrylate (BMA), dodecyl methacrylate (LMA) and oxiran-2-ylmethyl methacrylate (GMA). Using NHN **A1** or NHN **C**, all reactions yielded polymers of controlled dispersity ($Đ = 1.19–1.46$) at moderate to high conversions (>82%), and the initiator efficiencies were kept above 100% (Table 2, entries 1–7). Compared to MMA, DMAEMA is more prone to polymerization and more light-sensitive, resulting in higher conversion using NHN **C**. Ethyl $\alpha$-iodophenylacetate (Eph-I) also worked well with various monomers, realizing low dispersity ($Đ = 1.21–1.44$) at moderate to high conversions (>78%) and high initiator efficiency ($I^* = 107\%–148\%$) (Table 3, entries 1–8). The initiator efficiency exceeding 100% suggests that the initiator has initiated more than one chain, resulting in a molecular weight smaller than expected theoretically. Taking the example of Table 2, entry 1, the polymer was analyzed through $^1$H NMR spectroscopy (Fig. S8 in Supporting information), showing the integral of the initiator and iodine chain end was not 1/1 (3.83/3). Nevertheless, the polymers produced with MMA express high chain end functionality, the successful production of these block copolymers serves as compelling evidence of the exceptional chain fidelity of PMMA-I. The polymer produced with MMA obtained at 3 h was analyzed, after purification through $^1$H NMR spectroscopy (Fig. 3). The methyl protons (a, a', and a") present in the side chain exhibited signals between 3.55 and 3.77 ppm. Further analysis revealed that the main peak observed at 3.55 ppm–3.62 ppm, along with its shoulder peak at 3.62–3.64 ppm, could be attributed to the monomer units (a) located in the middle of the polymer chain. Additionally, a smaller

**Table 2**
Investigations on the monomer scope with CP-I.[a]

| Entry | Monomer | Conv. (%)[b] | $M_{n,GPC}$ (g/mol)[c] | $M_{w,GPC}$ (g/mol)[c] | $Đ$ ($M_w/M_n$)[c] | $I^*$ (%)[d] |
|---|---|---|---|---|---|---|
| 1 | MEMA | >99 | 23,100 | 27,500 | 1.19 | 126 |
| 2 | BnMA | 95 | 23,600 | 28,100 | 1.19 | 142 |
| 3 | PhMA | 82 | 19,300 | 25,100 | 1.30 | 139 |
| 4 | EHMA | 86 | 22,200 | 26,200 | 1.18 | 155 |
| 5 | BMA | 97 | 24,000 | 29,100 | 1.21 | 115 |
| 6 | GMA | 98 | 21,700 | 28,500 | 1.31 | 129 |
| 7[e] | DMAEMA | >99 | 23,200 | 33,800 | 1.46 | 136 |

[a] Reaction conditions: NHN **A1** was used as the catalyst, bulk polymerization, [Monomer]:[CP-I]:[NHN] = 200:1:0.2, room temperature, 455 nm LED (2 W), 24 h.
[b] Monomer conversion measured by $^1$H NMR.
[c] Molecular weights and molecular weight distributions were determined by GPC using PMMA as the standard in THF.
[d] $I^* = M_{n,theo}/M_{n,GPC}$, $M_{n,theo} = MW_{CP-I} + 200 \times MW_{Monomer} \times$ Conversion%.
[e] NHN **C** was used as the catalyst.

**Table 3**
Investigations on the monomer scope with Eph-I.[a]

| Entry | Monomer | Conv. (%)[b] | $M_{n,GPC}$ (g/mol)[c] | $M_{w,GPC}$ (g/mol)[c] | $Đ$ ($M_w/M_n$)[c] | $I^*$ (%)[d] |
|---|---|---|---|---|---|---|
| 1 | MEMA | >99 | 27,300 | 33,100 | 1.21 | 107 |
| 2 | EHMA | 90 | 25,500 | 32,500 | 1.27 | 141 |
| 3 | BnMA | 92 | 22,500 | 28,000 | 1.24 | 148 |
| 4 | PhMA | 81 | 19,100 | 24,600 | 1.29 | 139 |
| 5 | GMA | 96 | 19,200 | 25,600 | 1.33 | 144 |
| 6[e,f] | LMA | >99 | 22,600 | 28,100 | 1.24 | 114 |
| 7[f] | DMAEMA | >99 | 24,900 | 34,900 | 1.40 | 127 |
| 8[f] | TFEMA | 78 | 19,100 | 27,500 | 1.44 | 139 |

[a] Reaction conditions: NHN **A1** was used as the catalyst, bulk polymerization, [Monomer]:[Eph-I]:[NHN]=200:1:0.2, room temperature, 455 nm LED (2 W), 24 h.
[b] Monomer conversion measured by $^1$H NMR.
[c] Molecular weights and molecular weight distributions were determined by GPC using PMMA as the standard in THF.
[d] $I^* = M_{n,theo}/M_{n,GPC}$, $M_{n,theo} = MW_{Eph-I} + [Monomer]/[Eph-I] \times MW_{Monomer} \times$ Conversion%.
[e] [Monomer]:[Eph-I]:[NHN] = 100:1:0.2.
[f] NHN **B** was used as the catalyst.

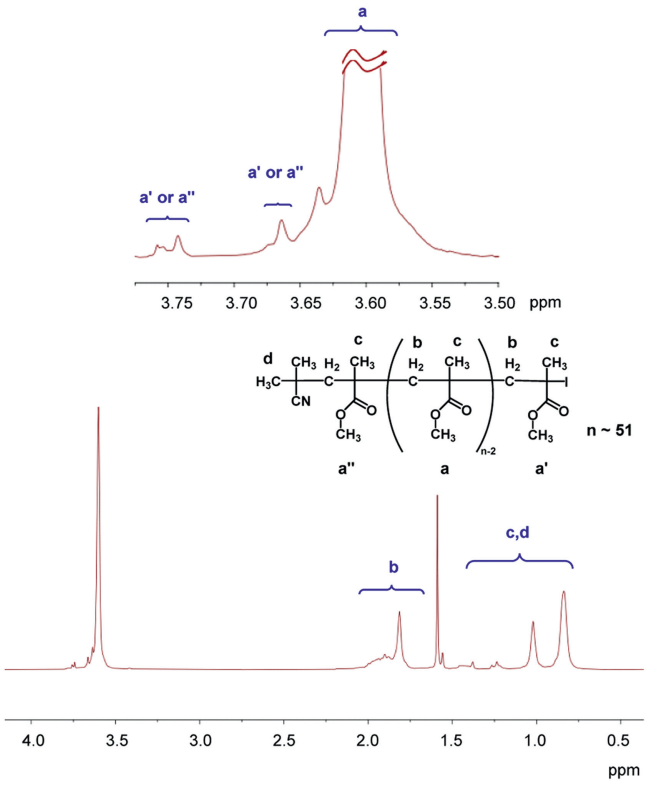


**Fig. 3.** $^1$H NMR spectrum (in $CDCl_3$) of PMMA-I ($M_n = 5300$, $Đ = 1.19$) after 3 h under the polymerization conditions of [MMA]:[CP-I]:[NHN **A1**] = 200:1:0.2, room temperature, 455 nm LED (2 W), bulk polymerization for 3 h.

peak at 3.73–3.77 ppm was identified and associated with the $\omega$-terminal chain-end unit (a') located next to the iodine. Another peak detected at 3.64–3.66 ppm originated from the $\alpha$-terminal chain-end unit (a'') situated adjacent to the 2-cyanopropyl (CP) group. However, this assignment is not definitive, and the peak at 3.64−3.66 ppm could also be assigned to the $\omega$-terminal chain-end unit (a') [40,76]. These findings indicate a well-controlled polymerization process.

We also performed block copolymerization. Initially, we synthesized PMMA-I, which exhibited a predetermined molecular weight and narrow molecular weight distributions, with the reaction running for 3 h. The resulting purified macroinitiator displayed two variants, one with $M_n$ of 5300 g/mol and $Đ$ of 1.19 presented in Fig. 4, and the other with $M_n$ of 4100 g/mol and $Đ$ of 1.21 presented in Fig. S7 (Supporting information). These purified macroinitiators were then utilized in the polymerization of GMA and BnMA. As depicted in Figs. 4A-C, we successfully synthesized block copolymers of PMMA-*b*-PGMA and PMMA-*b*-PBnMA with remarkable conversions of 95% and 91%, respectively. The successful production of these block copolymers serves as compelling evidence of the exceptional chain fidelity of PMMA-I.

Our previous experimental studies have shown that NHN cation can form photoactive CTCs with $I^-$ anion (see Supporting information for details) [60–65]. Under blue light irradiation, the CTC undergoes single electron transfer (SET), giving NHN aminyl radical (NHN$^\bullet$) and iodide radical ($I^\bullet$). We further performed density functional theory (DFT) calculations (see Supporting information for computational details) to understand the polymerization mechanism. Fig. 5 shows the results for NHN$^\bullet$ to activate the initiator CP-I. The activation crosses a transition state **$^2$TS1**, resulting in alkyl radical **$^2$IM1** and meanwhile regenerating NHN **A1**. The activation is exergonic by 20.8 kcal/mol with a barrier of 9.7 kcal/mol, thus the initiation of the polymerization is facile (Fig. 5A, left). We further analyzed how NHN$^\bullet$ activates CP-I (Fig. 5B). Along the intrinsic reaction coordinate (IRC) from the reactant- to product-side, the charge on I atom increases to approach to -1.0 e, while the spin population of N-N-N moiety decreases rapidly to approach to 0.0. The charge and spin population evolutions clearly indicate the transfer of an electron from NHN$^\bullet$ to CP-I. The charge and spin population change rapidly around the **$^2$TS1**, suggesting the single electron transfer takes place around the transition state. In addition, along IRC, the C-I bond is gradually elongated, while the N-I distance becomes shorter prior to **$^2$TS1** and then increases slowly. The activation does not form N-I bond, because the cationic NHN prefers forming a salt with iodide anion ($I^-$), rather than a covalent compound with iodide. Frontier molecular orbital (FMO) analysis (Fig. 5A, right) shows that **$^2$TS1** exhibits significant orbital interaction between the singly occupied molecular orbital (SOMO) of

A. Block Copolymerizations[a]

| Entry | Macroinitiator | Monomer | Conv. (%)[b] | $M_{n,GPC}$[c] (g/mol) | $M_{w,GPC}$[c] (g/mol) | $Đ$[c] ($M_w/M_n$) | $I^*$ (%)[d] |
|---|---|---|---|---|---|---|---|
| 1 | PMMA-I[e] | GMA | 95 | 24700 | 34600 | 1.40 | 126 |
| 2 | PMMA-I[f] | BnMA | 91 | 36800 | 49500 | 1.35 | 101 |

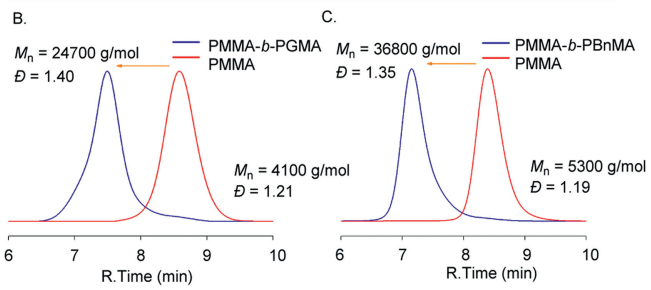


**Fig. 4.** (A) Conditions: [a]Under simulated blue light irradiation (using a blue LED with an output optical power of 2 W and a wavelength of 455 nm) at ambient temperature, NHN **A1** was used as the catalyst, bulk polymerization, 24 h. [Monomer]:[PMMA-I]:[NHN] = 200:1:0.2. [b] Monomer conversion measured by $^1$H NMR. [c] Molecular weights and molecular weight distributions were determined by GPC using PMMA as the standard in THF. [d] $I^* = M_{n,theo}/M_{n,GPC}$, $M_{n,theo} = M_{n,PMMA-I} + 200 \times MW_{monomer} \times$ Conversion%. [e] $M_n = 4100$ g/mol and $Đ = 1.21$ for PMMA–I. [f] $M_n = 5300$ g/mol and $Đ = 1.19$ for PMMA–I. (B) GPC traces of PMMA-*b*-PGMA copolymerization. (C) GPC traces of PMMA-*b*-PBnMA copolymerization.

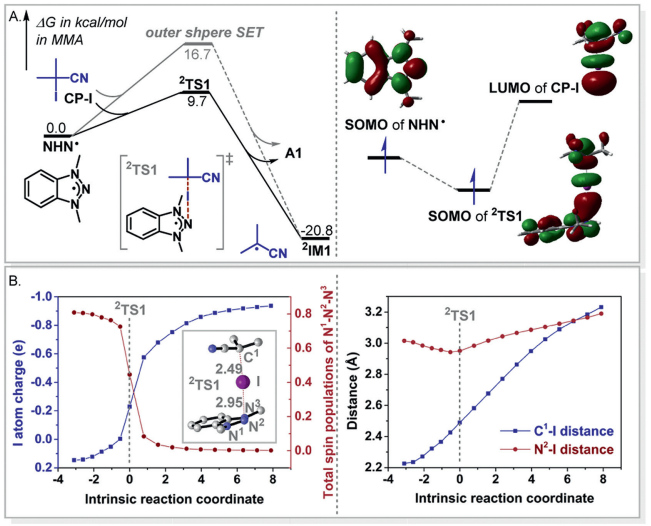


**Fig. 5.** Computational characterization of the SET process between NHN$^\bullet$ radical and CP-I. (A) Comparing the energetics of NHN$^\bullet$ to activate CP-I *via* ISET and OSET, respectively. Orbital interaction of singly occupied molecular orbital (SOMO) of NHN$^\bullet$ with the C-I $\sigma$-antibonding orbital of CP-I. (B) evolutions of the charge, spin population, N-I and C-I bond lengths, along the intrinsic reaction coordinate (IRC) starting with **$^2$TS1**. Hydrogen atoms in the geometry of **$^2$TS1** are omitted for clarity.

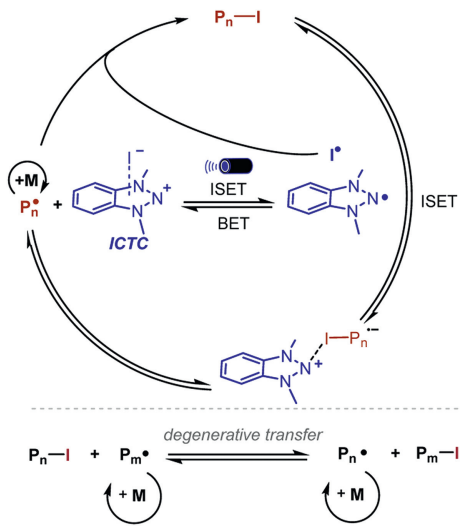


**Fig. 6.** Proposed mechanism.

NHN• and the C-I $\sigma$-antibonding orbital, which facilitates the C-I bond cleavage, thus aiding the SET from NHN• to CP-I. Indeed, the barrier (9.7 kcal/mol) for the ISET *via* **$^2$TS1** is much lower than that (16.7 kcal/mol, predicted with Marcus electron transfer theory (see Supporting information for details)) for the OSET from NHN• to CP-I (Fig. 5A, left). The ISET feature benefits the selective activation of the C-I bond of CP-I, thus disfavoring possible side reactions. This could be an advantage of our strategy, because it avoids strongly oxidizing PC•$^+$ involved in the iodine-mediated RDRP enabled by photoredox catalysts. The above analyses hold true for the generation of $P_n$• radical *via* the reduction of $P_n$-I with NHN• (Fig. S17 in Supporting information).

Subsequent to the initiation, the resultant radical **$^2$IM1** adds to MMA to start chain propagation. As shown in Fig. S18 (Supporting information), the subsequent MMA additions are nearly thermodynamically neutral with barriers less than 20.0 kcal/mol. The kinetics and thermodynamics account for the controlled polymerization.

According to the computational results, we elaborated a catalytic cycle for the polymerization in Fig. 6. Under light irradiation, the NHN$^+$···I$^-$ salt undergoes SET, giving NHN• and I• radicals. The NHN• radical initiates the activator CP-I or dormant $P_n$-I *via* an inner-sphere SET process, resulting in the propagating $P_n$• radical and regeneration of the catalyst NHN$^+$···I$^-$. The $P_n$• radical can add to MMA to grow the chain, giving $P_{n+m}$• radical. The coupling of I• and $P_{n+m}$• converts to $P_{n+m}$-I, which can be initiated by NHN•···I• to continue growth when light is on or the polymerization product when light is off. Essentially, the polymerization continuously exchanges the I atom in $P_n$-I and the I atom in NHN$^+$···I$^-$ through light irradiation, which makes our approach simple and straightforward without using an additional electron donor. However, due to the easy cleavage of $P_n$-I bond, a competitive degenerative transfer (DT) process between the growing radicals and iodine-capped dormant species is inevitable [40,41,77,78] which influences the control over polymer chain growth. Comparing the photoinduced NHN-catalyzed process in Fig. 6 and the RCMP process in Fig. 1B, a mechanistic difference between them lies on how the dormant $P_n$-I is activated. In RCMP, the $P_n$-I·catalyst complex undergoes homolytic C-I bond cleavage upon light irradiation, while the $P_n$-I bond in our process is activated *via* ISET reduction with the *in situ* formed NHN radical.

In summary, we have demonstrated that photoactive NHN$^+$···I$^-$ charge transfer complex is effective for iodine-mediated RDRP without using any additive. In this approach, the NHN$^+$···I$^-$ salt undergoes a SET under light irradiation, generating NHN• and I• radicals. The NHN• radical could activate the dormant $P_n$-I polymer through an inner-sphere SET process, leading to the propagating $P_n$• radical and an I$^-$ for recovering the salt. The coupling of $P_n$• and I• radicals deactivate the polymerization to give the polymerization product. This method is simple and robust and can perform iodine-mediated RDRP with various methacrylate-based monomers, producing well-controlled polymers. In addition, the method features desirable characteristics such as being additive-free and the ready availability of the NHN salts. We anticipate that the CTC-based strategy could inspire further advancements in this field.

## Declaration of competing interest

The authors declare that they have no known competing financial interests or personal relationships that could have appeared to influence the work reported in this paper.

## CRediT authorship contribution statement

**Xiang Li:** Writing – original draft, Methodology, Data curation. **Beibei Zhang:** Software, Data curation. **Zhixiang Wang:** Writing – review & editing, Writing – original draft, Supervision, Software, Project administration, Funding acquisition. **Xiangyu Chen:** Writing – review & editing, Writing – original draft, Supervision, Project administration, Funding acquisition.

## Acknowledgments

Supported by the National Natural Science Foundation of China (Nos. 21773240 and 22173103), the University of the Chinese Academy of Sciences and Beijing National Laboratory for Molecular Sciences (No. BNLMS2023014).

## Supplementary materials

Supplementary material associated with this article can be found, in the online version, at doi:10.1016/j.cclet.2024.110383.

## References

[1] W.A. Braunecker, K. Matyjaszewski, Prog. Polym. Sci. 32 (2007) 93–146.
[2] A.D. Jenkins, R.G. Jones, G. Moad, Pure Appl. Chem. 82 (2009) 483–491.
[3] K. Matyjaszewski, N.V. Tsarevsky, Nat. Chem. 1 (2009) 276–288.
[4] D.A. Shipp, Polym. Rev. 51 (2011) 99–103.
[5] N. Corrigan, K. Jung, G. Moad, et al., Prog. Polym. Sci. 111 (2020) 101311–101337.
[6] A.D. Asandei, Chem. Rev. 116 (2016) 2244–2274.
[7] M. Chen, M. Zhong, J.A. Johnson, Chem. Rev. 116 (2011) 10167–10211.
[8] C. Wu, N. Corrigan, C.H. Lim, et al., Chem. Rev. 122 (2022) 5476–5518.
[9] M. Destarac, Polym. Chem. 9 (2018) 4947–4967.
[10] A.M. Braun, L. Jakob, E. Oliveros, et al., Adv. Photochem. 18 (1993) 235–313.
[11] C. Deng, Y. Lin, Y. Huang, et al., Green Synth. Catal. (2023), doi:10.1016/j.gresc.2023.11.009.
[12] N.A. Romero, D.A. Nicewicz, Chem. Rev. 116 (2016) 10075–10166.
[13] B.P. Fors, C.J. Hawker, Angew. Chem. Int. Ed. 51 (2012) 8850–8853.
[14] E.H. Discekici, A. Anastasaki, J. Read de Alaniz, et al., Macromolecules 51 (2018) 7421–7434.
[15] G. Yilmaz, Y. Yagci, Polym. Chem. 9 (2018) 1757–1762.
[16] D.A. Corbin, G.M. Miyake, Chem. Rev. 122 (2022) 1830–1874.
[17] Z. Wu, C. Boyer, Adv. Sci. 10 (2023) 2304942.
[18] Q. Ti, L. Fang, W. Zhao, et al., J. Am. Chem. Soc. 145 (2023) 26160–26168.
[19] H. Zhou, L. Zhang, P. Wen, et al., Angew. Chem. Int. Ed. 62 (2023) e202304461.
[20] X. Hu, R. Yin, J. Jeong, et al., J. Am. Chem. Soc. 146 (2024) 13417–13426.
[21] J. Jeong, X. Hu, R. Yin, et al., J. Am. Chem. Soc. 146 (2024) 13598–13606.
[22] Y. Zhang, H. Wang, D. Jiang, et al., Green Synth. Catal. 5 (2024) 35–41.
[23] G.M. Miyake, J.C. Theriot, Macromolecules 47 (2014) 8255–8261.
[24] N.J. Treat, H. Sprafke, J.W. Kramer, et al., J. Am. Chem. Soc. 136 (2014) 16096–16101.
[25] R.M. Pearson, C.H. Lim, B.G. McCarthy, et al., J. Am. Chem. Soc. 138 (2016) 11399–11407.
[26] J.C. Theriot, C.H. Lim, H. Yang, et al., Science 352 (2016) 1082–1086.
[27] C.K. Prier, D.A. Rankic, D.W.C. MacMillan, Chem. Rev. 113 (2013) 5322–5363.
[28] M.H. Shaw, J. Twilton, D.W.C. MacMillan, J. Org. Chem. 81 (2016) 6898–6926.
[29] D. Corbin, C.H. Lim, G. Miyake, Aldrichimica Acta 52 (2019) 7–21.

[30] G. Zhang, I.Y. Song, K.H. Ahn, et al., Macromolecules 44 (2011) 7594–7599.
[31] X. Liu, L. Zhang, Z. Cheng, et al., Polym. Chem. 7 (2016) 689–700.
[32] J.S. Wang, K. Matyjaszewski, J. Am. Chem. Soc. 117 (1995) 5614–5615.
[33] J.S. Wang, K. Matyjaszewski, Macromolecules 28 (1995) 7901–7910.
[34] M. Kato, M. Kamigaito, M. Sawamoto, et al., Macromolecules 28 (1995) 1721–1723.
[35] Y.Y. Yang, P. Zhang, N. Hadjichristidis, J. Am. Chem. Soc. 145 (2023) 12737–12744.
[36] K. Matyjaszewski, J. Xia, Chem. Rev. 101 (2001) 2921–2990.
[37] Y. Ni, L. Zhang, Z. Cheng, et al., Polym. Chem. 10 (2001) 2504–2515.
[38] S. Lanzalaco, M. Fantin, O. Scialdone, et al., Macromolecules 50 (2017) 192–202.
[39] A. Ohtsuki, A. Goto, H. Kaji, Macromolecules 46 (2013) 96–102.
[40] A. Ohtsuki, L. Lei, M. Tanishima, et al., J. Am. Chem. Soc. 137 (2015) 5610–5617.
[41] C.G. Wang, C. Chen, K. Sakakibara, et al., Angew. Chem. Int. Ed. 57 (2018) 13504–13508.
[42] C.G. Wang, A.M.L. Chong, H.M. Pan, et al., Polym. Chem. 11 (2020) 5559–5571.
[43] Y. Ni, C. Tian, L. Zhang, et al., ACS Macro Lett. 8 (2019) 1419–1425.
[44] C. Tian, P. Wang, Y. Ni, et al., Angew. Chem. Int. Ed. 59 (2020) 3910–3916.
[45] S. DadashiSilab, G. Szczepaniak, S. Lathwal, et al., Polym. Chem. 11 (2020) 843–848.
[46] Q. Wang, F.Y. Bai, Y. Wang, et al., J. Am. Chem. Soc. 144 (2022) 19942–19952.
[47] H. Sheng, Q. Liu, F. Chen, et al., Chin. Chem. Lett. 33 (2022) 4298–4302.
[48] X.J. Ren, Q. Liu, Z.X. Wang, et al., Chin. Chem. Lett. 34 (2023) 107473.
[49] X.J. Ren, Q. Liu, Z.S. Yang, et al., Chin. Chem. Lett. 34 (2023) 107821.
[50] S. Qiao, K.Q. Chen, Q. Liu, et al., Chin. Chem. Lett. 35 (2024) 108979.
[51] Y. Tulchinsky, M.A. Iron, M. Botoshansky, et al., Nat. Chem. 3 (2011) 525–531.
[52] A. Pogoreltsev, Y. Tulchinsky, N. Fridman, et al., J. Am. Chem. Soc. 139 (2017) 4062–4067.
[53] J. Zhou, L.L. Liu, L.L. Cao, et al., Angew. Chem. Int. Ed. 57 (2018) 3322–3326.
[54] I. Avigdori, A. Pogoreltsev, A. Kaushanski, et al., Angew. Chem. Int. Ed. 59 (2020) 23476–23479.
[55] A. Koronatov, A. Mauda, B. Tumansky, et al., J. Am. Chem. Soc. 144 (2022) 23642–23648.
[56] M. Mehta, J.M. Mehta, Angew. Chem. Int. Ed. 59 (2020) 2715–2719.
[57] T. Danelzik, S. Joseph, C. Mück-Lichtenfeld, et al., Org. Lett. 24 (2022) 6105–6110.
[58] D. Ranolia, I. Avigdori, K. Singh, et al., Org. Lett. 24 (2022) 3915–3919.
[59] K. Singh, I. Avigdori, A. Kaushansky, et al., ACS Catal. 12 (2022) 6831–6839.
[60] K.Q. Chen, B.B. Zhang, Z.X. Wang, et al., Org. Lett. 24 (2022) 4598–4602.
[61] L. Bao, Z.X. Wang, X.Y. Chen, Org. Lett. 25 (2023) 565–568.
[62] X.J. Ren, P.W. Liao, H. Sheng, et al., Org. Lett. 25 (2023) 6189–6194.
[63] X.D. Su, Z.S. Yang, W. Gong, et al., Org. Chem. Front. 10 (2023) 1160–1165.
[64] C.S. Zhang, C.Z. Fang, L. Yi, et al., Org. Chem. Front. 11 (2024) 673–683.
[65] C.S. Zhang, K.Q. Chen, L. Zhou, et al., Org. Chem. Front. 11 (2024) 2070–2074.
[66] H. Zhao, H. Li, C. Tian, et al., Macromol. Rapid Commun. 42 (2021) 2100211.
[67] S. Ren, H. Li, X. Xu, et al., Biomater. Sci. 11 (2023) 509–517.
[68] S. Chen, M. Yang, H. Li, et al., Eur. Polym. J. 186 (2023) 111850.
[69] S. Ren, X. Xu, J. Sun, et al., Eur. Polym. J. 195 (2023) 112232.
[70] H. Zhao, G. Bian, X. Xu, et al., Macromolecules 56 (2023) 6328–6338.
[71] L. Xiao, Q. Li, Y. Liu, et al., Polym. Chem. 12 (2021) 6714–6723.
[72] Q. Li, Z. Lu, H. Yang, et al., Polym. Chem. 13 (2022) 527–535.
[73] Z. Lu, R. Zhao, H. Yang, et al., Angew. Chem. Int. Ed. 6 (2022) e202208898.
[74] Y.N. Li, S.Y. Zhang, Y. Ma, et al., ACS Catal. 12 (2022) 11606–11614.
[75] Z.H. Chen, X.Y. Wang, Y. Tang, Polym. Chem. 13 (2022) 2402–2419.
[76] A. Goto, H. Ohfuji, M. Tanishima, J. Am. Chem. Soc. 135 (2013) 11131–11139.
[77] K. Koumura, K. Satoh, M. Kamigaito, Macromolecules 41 (2008) 7359–7367.
[78] A.D. Asandei, O.I. Adebolu, C.P. Simpson, J. Am. Chem. Soc. 134 (2012) 6080–6083.